Photoemission and STM Study of the Morphology and Barrier Heights at the Interface between Perylene and Noble Metal (111) Surfaces

ARTICLE *in* THE JOURNAL OF PHYSICAL CHEMISTRY C · AUGUST 2010

Impact Factor: 4.77 · DOI: 10.1021/jp1008626

2 AUTHORS:

Kedar Manandhar
University of Illinois at Chicago
20 PUBLICATIONS **90** CITATIONS

SEE PROFILE

Bruce A Parkinson
University of Wyoming
251 PUBLICATIONS **7,087** CITATIONS

SEE PROFILE

Morphologies, structures, and interfacial electronic structure of perylene on Au(111)

K. Manandhar,[1] J. B. Sambur,[2] and B. A. Parkinson[1,a)]
[1]*Department of Chemistry and School of Energy Resources, University of Wyoming, Laramie, Wyoming 82071, USA*
[2]*Department of Chemistry, Colorado State University, Fort Collins, Colorado 80523, USA*

(Received 30 July 2009; accepted 18 January 2010; published online 31 March 2010)

Various coverages of perylene thin films on Au(111) were investigated using scanning tunneling microscopy (STM) and ultraviolet photoelectron spectroscopy and x-ray photoelectron spectroscopy. A Schottky junction formed between Au(111) and perylene consisted of a large 0.65 eV interface dipole and a hole barrier height of 0.85 eV. A wetting layer of approximately 4 Å thickness was initially formed followed by island formation, consistent with Stranski–Krastanov growth. Room temperature STM investigations of nominal one monolayer perylene films revealed symmetry equivalent domains and two different stable commensurate lattice structures. Perylene film growth mode, film structure and the energy level diagram are discussed.
 [doi:10.1063/1.3318682]

I. INTRODUCTION

In recent years organic semiconductors have been intensively studied due to their successful application in electronic and optoelectronic devices. Devices such as organic light emitting diodes and organic thin film transistors have been demonstrated and their performance has rapidly improved.[1–3] These devices employ an organic-metal (OM) thin film architecture where the metals are electron or hole injection contacts. The OM interface plays an important role or even predominant role in those devices because the electrical and optical characteristics of OM contacts depend to a large extent on the energy barriers for injection of holes and electrons. It was initially assumed that OM interfaces followed Mott–Schottky limit, and thus the relevant carrier injection barriers could be predicted from the fundamental properties of the separate constituents (i.e., highly occupied molecular orbital (HOMO) and lowest unoccupied molecular orbital (LUMO) gap, and ionization potential (IP) of the semiconductor and work function of the metal). However, experiments performed on a wide variety of OM interfaces revealed a far more complex situation, where behavior ranged from the Schottky to Bardeen limit.[4–6] The basic phenomena, the physical and electronic properties of OM interfaces, which eventually determine charge carrier injection and transport into organic semiconductor films are not yet well understood. In order to improve future organic electronic and optoelectronic devices, understanding the fundamental factors that govern efficient charge injection and rectification at the OM interface must be determined.

Besides the barrier height related to the energy level difference between the frontier orbitals of the organic molecules at interfaces and the work function of the metal, the overlap of the wave functions of corresponding energy levels is important for establishment of the electrical and optical properties of the interface.[7] Since the spatial spread of the molecular wave function is in general not isotropic, the overlap depends on the orientation of the molecules in the thin film.[7] Enhanced field effect carrier mobilities, together with increased electrical conductivity and reduced activation energy for electrical conduction have been reported when the ordering of the organic thin film is improved.[8,9] Tsiper *et al.*[10] and Alvarado *et al.*,[11] using scanning tunneling microscopy and scanning tunneling spectroscopy (STM/STS), reported that the energy of charge carrier injection into thin films of 3,4,9,10-perylene-tetracarboxylicacid-dianhydride and copper phthalocyanine (CuPc), on Au(111) strongly depended on the intermolecular packing and crystallographic order of the thin films. As the degree of crystalline order of the thin film improved, the energy gap decreased and charge transport properties improved. Thus a detailed understanding of the adsorption process of organic molecules on metal substrates, which often yields interesting surface structures and packing motifs, are of prime importance.

Perylene, a D_{2h} symmetry polyaromatic hydrocarbon, attracted considerable interest because perylene thin films showed excellent electro-optical properties. A very high electron mobility of 5 cm^2/Vs along one of the orthogonal principal axes in a single crystal perylene film[12] and improved photovoltaic performance for perylene doped CuPc devices[13] has been demonstrated. Thin films of perylene have been studied on different metal and semiconductor surfaces including Au(111) (Refs. 14–16) and Cu(111).[17] Perylene adsorbs on these surfaces in a planer arrangement for coverages up to a monolayer (ML). A commensurate lattice with lattice vectors of 11.5×11.5 $Å^2$ was reported both by Gao *et al.*[15] at cryogenic temperatures using STM and Seidel *et al.*[16] using low energy electron diffraction (LEED). However Seidel *et al.* defined this as an intermediate structure since it transformed to a stable incommensurate structure with lattice vec-

a)Author to whom correspondence should be addressed. Present address: University of Wyoming, Department of Chemistry and School of Energy Resources, Laramie, WY 82071. Tel.: +1 307 766 4363. FAX: +1 307 766 2807. Electronic mail: bparkin1@uwyo.edu.

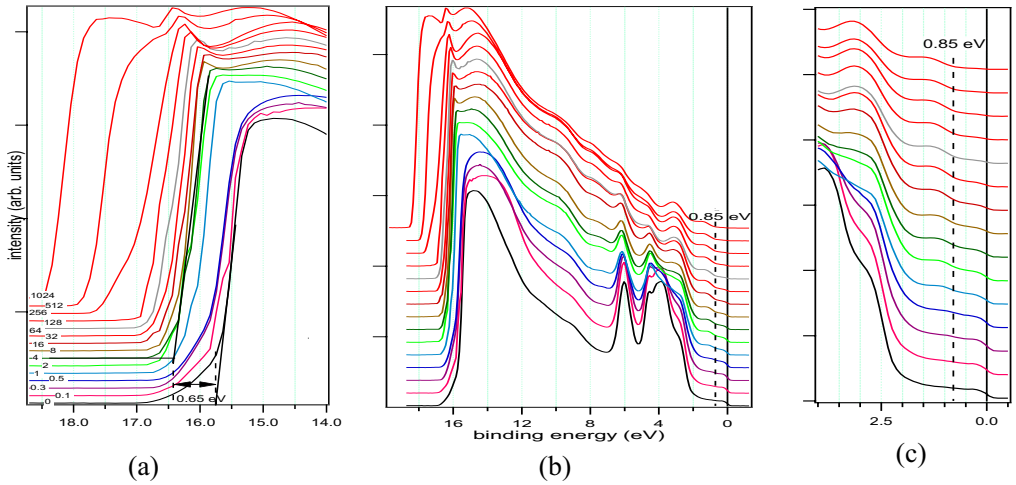

FIG. 1. (Color online) UPS HeI spectra of perylene. (a) HBEC region. (b) Full spectra. (c) HOMO range.

tors 10.6×12.2 Å^2. They proposed that perylene adopts a different packing arrangement that approaches the bulk structure for coverages above one ML on Au(111).[15] The similar five ring polyaromatic hydrocarbon pentacene forms many two-dimensional (2D) lattice structures at just below one ML coverages on Au(111).[18,19]

The relative position of perylene frontier orbitals the HOMO and the HOMO and the LUMO, with respect to Au(111) Fermi level has been measured using ultraviolet photoelectron spectroscopy (UPS) (Ref. 14) and STS,[15] respectively. The position of HOMO was about 1.0 eV below the gold Fermi level in both the cases. In this contribution, we report a measurement of the energy level alignment for perylene on Au(111) using x-ray photoelectron spectroscopy (XPS), UPS, and UV-Vis, and the packing structures formed at nominal one ML coverages.

II. EXPERIMENTAL

Experiments were performed in a commercial Omicron Multiprobe ultrahigh vacuum (UHV) system (base pressure 5×10^{-10} Torr). This system is equipped with a variable temperature STM (VT-STM) for surface structural characterization. XPS and UPS, using a VSW EA125 single channel hemispherical analyzer, were used to study the electronic structure of the interface. A physical vapor deposition chamber (base pressure 9×10^{-9} Torr) is attached to the UHV system allowing samples and films to be prepared *in situ*.

The gold film was prepared in a Denton DV-502 high vacuum evaporator by evaporating gold onto freshly cleaved mica. The film was approximately 400 Å thick. Cycles of sputtering at 1 keV energy with Ar-partial pressure of 1×10^{-6} Torr and annealing at 400 °C were used to clean and flatten the Au(111) surface. The chemical purity of the surface was determined with XPS (Mg kα, 50 eV pass energy) and the presence of the $23 \times \sqrt{3}$ reconstruction was confirmed with STM.[20] The surfaces revealed terraces as large as 350×240 nm^2 with mono-atomic step heights of 2.3 Å. In small area scanning, the hexagonal structure of the lattice was resolved with the measured lattice constant of 2.6 Å.

Perylene (Aldrich Chemical Co.) films were deposited under UHV (base pressure 9×10^{-9} Torr) using a silicone rubber flexible heater to resistively heat a quartz ampule with a UHV series quartz-metal adapter (source temperature, ~125 °C). The source was extensively degassed at about 102 °C prior to deposition. The quartz ampule containing perylene was heated to obtain a desired deposition rate that was monitored by a Leybold quartz crystal microbalance (QCM). The deposition rate was on average 1.5 ML/min with 1 ML is defined as a thickness of 4 Å as measured by the QCM. The Au(111) substrate was maintained at room temperature (RT) during the deposition.

Sequential depositions were performed up to a final film thickness of 1024 Å. After each growth step, XPS and UPS (HeI, 21.21 eV; with 10 eV pass energy) were utilized to measure the electronic structure of the surface. XPS spectra were taken with a takeoff angle of ≈20° of the normal emission, while UPS spectra were collected under normal emission. A −10.00 V bias was applied to the sample for the UPS measurements to separate the sample and spectrometer high binding energy cutoffs (HBECs). The spectrometer was calibrated as previously described.[21] Work function and HOMO-cutoff positions were determined from the HBECs and HOMO onsets respectively, of UP spectra. XPS core level peak positions were determined by fitting routine using IGOR PRO (Wavemetrics) data evaluation software. A vacuum deposited perylene film on quartz was used to obtain the thin film solid-state absorption spectrum that was measured using a Varian Cary–500 UV-Vis-NIR spectrophotometer.

STM was performed in constant current imaging mode using mechanically cut Pt/Ir tips with typical tip biases of −0.50 and −0.82 V and tunneling currents between 40 and 300 pA. All STM images were taken at RT. The Au(111) surface was renewed before each STM experiment with a sputter and anneal cycle. For STM experiment a nominal 1 ML of perylene was deposited onto the atomically clean Au(111) surface. The investigated perylene films were formed either by one-step or by two-step deposition. The one-step deposited overlayers were not heat treated after deposition whereas in the two-step deposited overlayers, a first sub-ML was annealed to 80 °C before adding a second half ML. The perylene molecular height, intermolecular distances, and lattice constants were calibrated using the *in situ*

measurements of hexagonal closed pack (hcp) and face centered cubic (fcc) domains with the characteristic $23\times\sqrt{3}$ herringbone reconstruction of Au(111) and also with the atomic resolution of Au(111) surface. The images were digitally filtered to remove low frequency noise and equalized using the WSXM software.[22]

III. RESULTS AND DISCUSSION

A. Interface dipole

The orbital energy alignment between Au(111) and perylene was measured utilizing photoemission spectroscopies. A clean Au(111) sample was prepared and characterized with both UPS and XPS. Perylene was then deposited in fourteen steps from clean Au(111) to a final thickness of 1024 Å. The HBEC region, complete HeI UPS spectra, and the HOMO spectral region as a function of perylene deposition are presented in Figs. 1(a)–1(c), respectively. Changes in the band structure are evident as the perylene film thickness increases. The existence of a large interface dipole is suggested by the significant shift in the HBEC [Fig. 1(a)] between the bare gold sample and the 4 Å thick perylene film. The work function of the gold substrate was determined by subtracting the HBEC of the UP spectra from the source energy (21.21 eV) yielding $\Phi=5.46$ eV. This work function is slightly higher than the published value of 5.31 eV for single crystal Au(111),[20] however a Au film on mica contains other Au orientations. Based on the observed multiterraced flat surfaces as large as 350×380 nm^2 in the scans of 500×500 nm^2 and $23\times\sqrt{3}$ herringbone reconstruction on the terraces and also hexagonal lattice structure on them in atomic resolution scan, we estimate that more than 53% surface of the gold film has (111) orientation. The work function of the film after deposition of 4 Å of perylene was determined to be 4.81 eV. The total work function shift of 0.65 eV calculated from the difference between the bare surface and the 4 Å deposition step represents the magnitude of the interface dipole formed by perylene on Au(111). This shift is about 0.55 eV larger than that reported by Kang *et al.*[14] for 8 Å perylene film on Au(111). The previous authors measured the smaller shift due to a 1.20 eV smaller value for their Au(111) surface work function, perhaps due to contamination of their Au surface. The shift in the work function as a function of perylene film thickness is plotted in Fig. 2(a).

B. Film growth mode

The C 1*s* spectra in Fig. 2(b) show that the C 1*s* BE for the small amount of contamination on the Au(111) surface is 284.78 eV.[4,5] After initial perylene deposition the BE gradually reduces to 284.50 eV at 4 Å thickness and remains unchanged within 0.05 eV up to a thickness of 512 Å. However at 1024 Å, the shift in the C 1*s* BE to 284.72 eV is due to the charging of perylene film.[5]

Figure 2(d) shows the normalized C 1*s* and Au 4*f* intensities as a function of coverage. The decrease in Au 4*f* and increase in C 1*s* intensity was most significant when the perylene thickness was 4 Å (Fig. 2(d) inset). The C 1*s* intensity was 20% of its eventual maximum whereas the Au 4*f* was 70% of its initial value [Fig. 2(d)]. The noticeable changes in intensities of the core level emissions at 4 Å of perylene, the constant BE of the C 1*s* core level emission starting at 4 Å and the significant change in the Au(111) work function between the bare gold and 4 Å of perylene [Fig. 2(a) inset] indicate that gold is uniformly covered with perylene at 4 Å. There is a decrease in the rate of change of intensities at intermediate coverages. The Au4f signal is still discernible after deposition of 1024 Å of perylene. This is most likely due to the formation of perylene islands. We therefore conclude that the growth mode for perylene on Au(111) follows the Stranski–Krastanov where an initial wetting layer is followed by island growth.

Figure 2

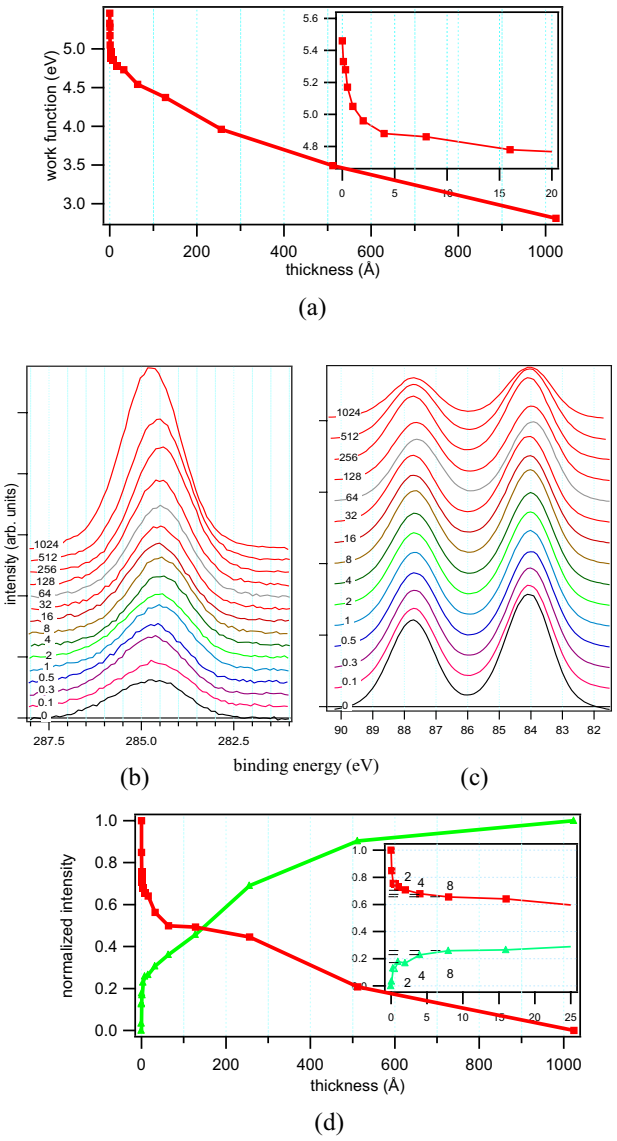

FIG. 2. (Color online) (a) A plot of work function of Au(111) vs perylene thickness. The inset is the plot for perylene thickness up to 20 Å. (b) and (c) are C 1*s* and Au 4*f* XPS spectra of 0–1024 Å thick perylene. (d) A plot of normalized intensity of C 1*s* (green curve with filled triangle) and Au 4*f* (red curve with filled square) vs perylene thickness. The inset is the plot for perylene thickness up to 25 Å.

C. Band bending and band diagram

Band bending occurring in the organic material, or polarization energy-related shifts at the interface were deter-

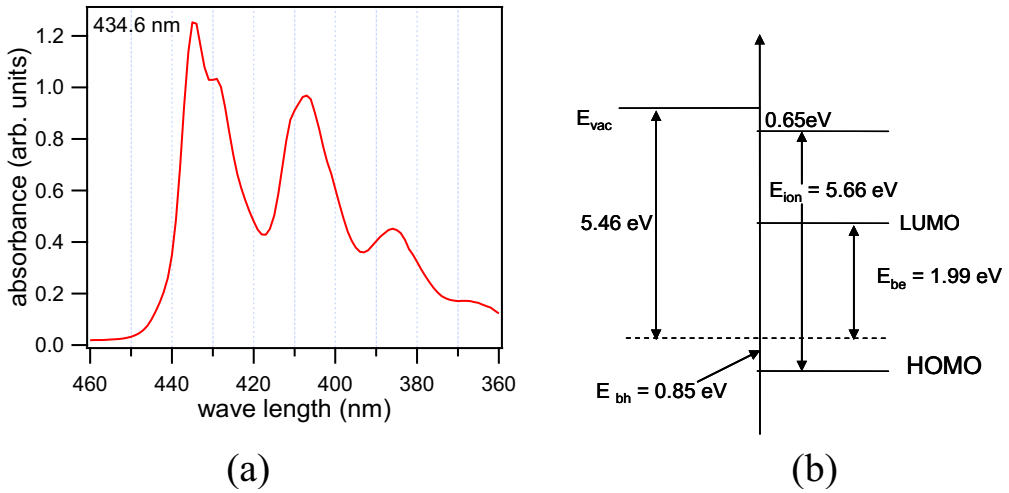

FIG. 3. (Color online) (a) Visible absorption spectrum of perylene. (b) Band diagram of perylene/Au(111).

mined by the measurement of the shift in the core level photoemission peaks. The Au 4*f* peaks are not subject to any band bending-related shifts and were constant at 84.00 eV after all deposition steps [Fig. 2(c)].[18] As previously discussed, there were no shifts in the C 1*s* core level BE related to perylene. The constant BE of the perylene emissions in UPS corroborate the C 1*s* core level XPS results, providing no evidence for band bending in the perylene films.

The HeI UPS spectra in Fig. 1 shows that subsequent depositions of the aromatic molecule results in the valence states of gold being gradually suppressed by the spectrum of the organic film. No states are observed at the Fermi energy (0 eV) however the HOMO of the perylene film is observed at the lowest BE edge of the spectrum with an onset at 0.85 eV. This value is about 0.10 eV smaller than that reported by Kang *et al.*[14] Again probably due to some contamination of their initial Au(111) surface. The energy difference between the gold Fermi level and the HOMO-cutoff of perylene is of interest because it represents the height of the hole injection barrier (E_{bh}) at the interface (E_{bh}=0.85 eV).

The position of the LUMO cannot be measured directly with XPS or UPS, however the perylene "band gap" can be estimated using the onset energy of optical absorption of a thin solid-state film of perylene. The visible absorption spectrum of a solid-state perylene film evaporated onto a quartz slide is shown in Fig. 3(a). The lowest energy absorption maximum occurs at 434.6 nm, corresponding to the first excitonic transition at 2.84 eV [Fig. 3(a)]. (It is important to note that the first excitonic transition is only used as an estimate for the HOMO-LUMO gap since the large excitonic BE of the molecules is not accounted for and results in an overestimate of the actual band gap.[23]) The estimated band gap for perylene allows for the determination of the energy level position of the perylene LUMO states with respect to the gold Fermi level by subtracting E_{bg} (2.84 eV) from E_{bh} (0.85 eV). This analysis yields the magnitude of the electron injection barrier for electrons to be injected into the organic material at the interface (E_{be}=1.99 eV). The IP of perylene was determined by adding the work function of the 4 Å perylene film (4.81 eV) to the HOMO cutoff (0.85 eV) of the same spectra, yielding 5.66 eV. All of these energy values are an estimate of the band line up for perylene on Au(111) since these measurements do not include the polarization related shifts. This information is graphically summarized in the energy alignment diagram of Fig. 3(b). It is worth noting that at approximately ML coverage, similar planner molecules pentacene and naphtho[2,3-a]pyrene which lay flat on Au(111) surface exhibit higher interface dipole (0.22 and 0.21 eV, respectively) than that measured on perylene/Au(111) interface.[21,23] In addition, these interfaces also exhibit a 0.30 eV smaller hole injection barrier than that for perylene. The optical HOMO-LUMO gap of perylene is larger than pentacene and naphtho[2,3-a]pyrene leading to 0.79 and 0.17 eV larger electron injection barrier, respectively.

D. Perylene surface structures

Scanning tunneling microscopy was utilized to image the morphology and structures of near ML perylene coverages on Au(111). Only noisy images were obtained at sub-ML coverages due to the perylene molecular motion at RT being faster than the time scale of the STM imaging process.[24–26] Well ordered close packed films are formed at near one ML coverages [Fig. 6(a)]. This observation is consistent with the highly mobile nature of a majority of polycyclic hydrocarbon (PAH) molecules on metal surfaces near RT.[24,26–28] However if the coverage is sufficiently high, the molecules are locked into ordered regions and form larger islands that can be imaged by the STM tip.[24,26,27]

Well ordered regions were also observed when the coverage increased (to make total coverage 1 ML nominal) onto a sub-ML covered surface at RT which was previously annealed at about 80 °C [Fig. 4(a)]. It is well known that sufficiently high surface mobility is required for diffusing species to nucleate.[29–31] The disordered molecules which formed islands upon mild annealing are still very small so they were easily disrupted by the STM tip. However these small islands may act as nucleation sites for larger island growth[32] when additional molecules are deposited.

As previously observed for other aromatic adsorbates[18,19,33] perylene does not lift the Au(111) $23\times\sqrt{3}$ reconstruction. The elevated herringbone reconstruction can

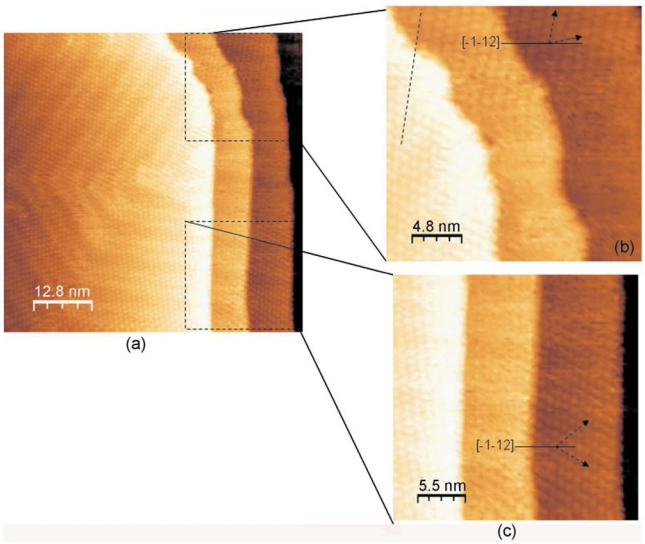

FIG. 4. (Color online) STM images of two-step deposited perylene film on Au(111). (−0.81 V, 40 pA). The top (24.1×24.1 nm^2) and bottom (27.2×27.2 nm^2) right are the zoomed-in images of the black-square sections shown in the left image (64.3×64.3 nm^2).

be seen through the organic film in the STM images in Figs. 4–6. The corrugation on the reconstructed surfaces is reflected in the cross-section [Fig. 5(b)] along the line in Fig. 5(a). The surface corrugation is due to the two alternating domains of hcp and fcc stacking of Au atoms[20,34] on the reconstructed gold surface. For the typical range of tunneling conditions used in this study, the corrugation is measured to be 0.14 Å, in agreement with the value measured by others.[20,34] The reconstruction traverses across the ordered perylene domain and reconstruction elbows are clearly visible at the top of the Fig. 5(a) and in the middle of the Fig. 4(a), which facilitates the determination of the $\langle 1\bar{1}2\rangle$ direction of the Au(111) substrate.

Large area scans (as large as of 247×247 nm^2) at multiple sites in the sample show that the entire surface is covered with molecules. The high resolution scan (Fig. 4(a)) of a 4 Å film clearly shows a well packed array of molecules over the entire surface. This observation is consistent with the UPS and XPS data at 4 Å coverage, where noticeable

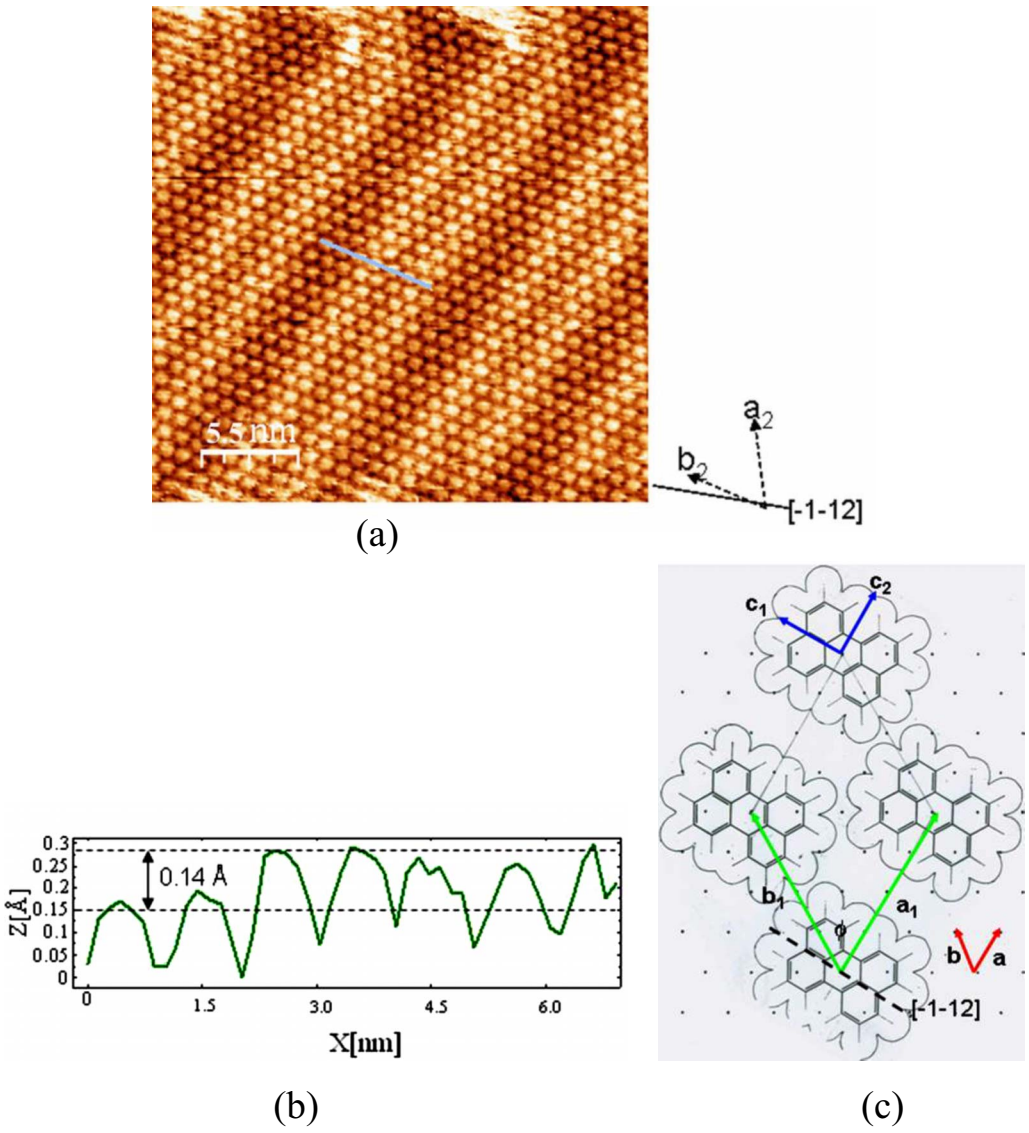

FIG. 5. (Color online) (a) STM image of two-step deposited perylene film on Au(111) (27.5×27.5 nm^2, −0.81 V, 40 pA). (b) The line profile along the line in (a). (c) A model showing structure of perylene in a unit lattice of (a). Blue arrows $\mathbf{c}_1$ and $\mathbf{c}_2$ are molecular axes, green arrows $\mathbf{a}_1$ and $\mathbf{b}_1$ are the overlayer lattice vectors, red arrows **a** and **b** are the substrate lattice vectors, dashed black line is the $\langle 1\bar{1}2\rangle$ direction of the substrate.

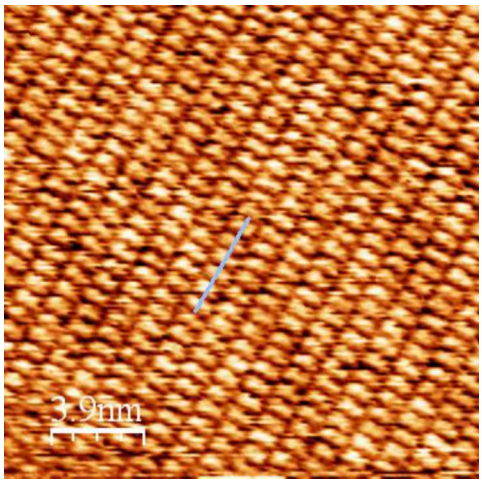

(a)

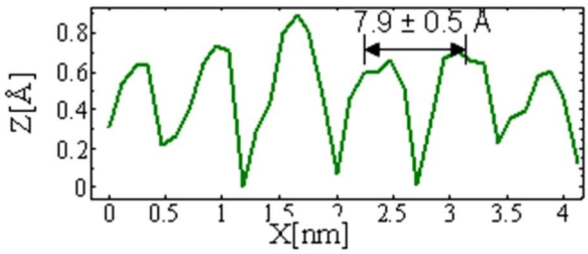

(b)

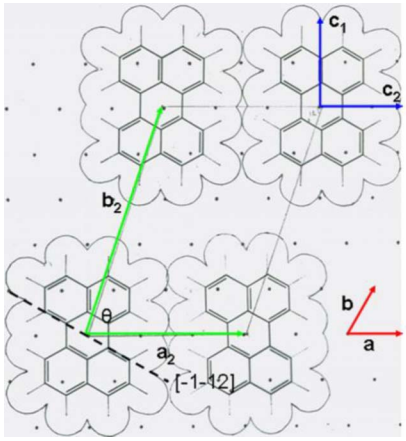

(c)

FIG. 6. (Color online) (a) STM image of one-step deposited perylene film on Au(111) (19.6×19.6 nm^2, -0.81 V, 51 pA). (b) The line profile along the line in (a). (c) A model showing structure of perylene in a unit lattice of (a). Blue arrows $\mathbf{c}_1$ and $\mathbf{c}_2$ are molecular axes, green arrows $\mathbf{a}_2$ and $\mathbf{b}_2$ are the overlayer lattice vectors, red arrows $\mathbf{a}$ and $\mathbf{b}$ are the substrate lattice vectors, dashed black line is the $\langle\bar{1}\bar{1}2\rangle$ direction of the substrate.

changes in the intensity of core level emissions compared to the bare surface, unchanged BE of C $1s$ core level emissions and significant changes of Au(111) work function between the bare gold were observed.

Figure 4(a) shows a multi-terraced surface of 64.3×64.3 nm^2 with ordered perylene molecules. The surface has one wide and two narrow terraces where the wide terrace has two perylene domains with the domain boundary running along the kinks in the $\langle\bar{1}\bar{1}2\rangle$ direction of the reconstructed surface. As seen in Fig. 4(a), the edges of the ordered domains slowly fade over the length of five to six molecules. We attribute this observation to the mobility of molecules at RT, where weakly bound molecules at the edge of a domain may detach from one site and subsequently diffuse across the surface and become reattached to another domain. Similarly, two domains are observed in the far-right-narrow terrace [Figs. 4(b) and 4(c)]. The domain in the lower part is rotated from the upper part of the terrace by $58°\pm4°$ [Figs. 4(b) and 4(c)]. The orientation between the domains reflects the rotational symmetry of the Au(111) substrate. The formation of such symmetry-equivalent domains has been reported for other PAH molecules on a surface with threefold rotational symmetry.[24,28,35,36]

A high resolution scan of the ordered region reveals that molecules are arranged in a 2D oblique lattice [Fig. 5(a)]. In all the domains the lattice vectors were measured to be 11.2 ± 0.3 Å by 11.2 ± 0.3 Å and angle between them was $60°\pm2°$ (Table I). The overlayer lattice vectors are related through the transformation equation $\begin{bmatrix}\mathbf{a}_1\\ \mathbf{b}_1\end{bmatrix}=\begin{bmatrix}4&0\\0&4\end{bmatrix}\begin{bmatrix}\mathbf{a}\\ \mathbf{b}\end{bmatrix}$, where $\mathbf{a}_1$ and $\mathbf{b}_1$ are the overlayer lattice vectors and $\mathbf{a}$ and $\mathbf{b}$ are the substrate lattice vectors. The whole numbers in the matrix refers to the commensurate super-structures that were previously reported for the perylene/Au(111) system.[15,16] The unit cell structure did not change while scanning for over one hour. The unit cell area is calculated as 16×7.08 Å^2 ≈114 Å^2 where 7.08 Å^2 is the substrate unit lattice area.

TABLE I. Experimentally measured lattice parameters and calculated lattice areas and Au atoms/perylene.

	1 step deposition	2 step deposition
|a| (Å)	8.5 ± 0.2	11.2 ± 0.3
|b| (Å)	12.9 ± 0.2	11.2 ± 0.3
∠(a,b) (°)	71 ± 1	60 ± 2
Lattice area (Å^2)	106	114
Au atoms/perylene	15	16

The density of perylene molecules on Au(111) is 8.77×10^{13} per cm^2 with 16 gold atoms per perylene molecule (Table I).

In the ordered layer formed from the single step deposition, a rectangular shaped individual perylene molecule is clearly observable [Fig. 6(a)]. The height profile of the molecule along the c_1 axis [Fig. 6(c)] (not presented here) is less than 0.05 Å, corresponding to a molecular tilt of about 0.3°. This confirms within experimental error that perylene molecules lie flat on the Au surface. The molecules form an oblique lattice with lattice vectors of 8.5 Å ± 0.2 Å [Fig. 6(b)] and 12.9 ± 0.2 Å with the angle between them of $71° \pm 1°$ [Fig. 6(c)]. The overlayer lattice vectors are related through the transformation equation by $\begin{bmatrix} \mathbf{a}_2 \\ \mathbf{b}_2 \end{bmatrix} = \begin{bmatrix} 3 & 0 \\ -1 & 5 \end{bmatrix} \begin{bmatrix} \mathbf{a} \\ \mathbf{b} \end{bmatrix}$ where the $\mathbf{a}_2$ and $\mathbf{b}_2$ are the overlayer lattice vectors and the $\mathbf{a}$ and $\mathbf{b}$ are the substrate lattice vectors [Fig. 6(c)]. This structure is commensurate with the unit lattice area calculated to be 15×7.08 Å$^2 \approx 106$ Å^2, where 7.08 Å^2 is the substrate unit lattice area (Table I). The density of perylene molecules is approximately 9.43×10^{13} cm^{-2} corresponding to 15 gold atoms per perylene molecule (Table I). This structure is slightly more densely packed than the one described above. Both structures correspond to the film of the first ML of perylene on Au(111), which dominate the interface dipole in the OM interface. The two structures are most likely present in different regions of the surface probed by the photoemission measurements. From the energy level diagram it is evident that the interface dipoles are pointing from molecules into the substrate resulting in a repulsive interaction between the molecules. The organic film lattice structures are the result of the delicate balance between the molecule-molecule and molecule-substrate interactions.[37] For the nominal 1 ML perylene films on Au(111), the lattice structures are commensurate which suggests that the film growth is largely determined by the substrate lattice. The growth may thus be characterized as van der Waals epitaxy.[37] Multiple 2D packing structures formed by aromatic molecules on metal surfaces is well known. For example on Au(111) pentacene shows at least nine different structures between 0.75 and 1.00 ML.[18,23,38] The multiple structures are a manifestation of the repulsive interactions of the molecules due to the strong interface dipole formed on the surface.

IV. CONCLUSIONS

We investigated thin films of perylene on Au(111) using UPS, XPS, and STM. The constant BE of C 1*s* core level emissions in XPS and perylene emissions in UPS provided no evidence of band bending in perylene-Au(111). The band line up of perylene on Au(111) illustrated that a Schottky barrier is formed between these materials with electron and hole injection barriers of 1.99 and 0.85 eV, respectively. An interface dipole of 0.65 eV was measured at the 4 Å perylene covered interface. The UPS and XPS spectra indicated that at approximately 4 Å thickness a wetting layer of perylene was formed followed by island growth. Under RT conditions no ordered domains were observed for sub-ML coverages presumably due to the highly mobile nature of the perylene molecules. For the nominal 1 ML coverages the film exhibited symmetry equivalent domains with molecules of the film laying flat on the surface. Two different stable and commensurate lattice structures with slightly different packing densities were found, a manifestation of the repulsive interactions of the molecules due to the strong interface dipole formed on the surfaces.

ACKNOWLEDGMENTS

This work was supported by NSF Grant No. CHE-0518563 and University of Wyoming startup funds.

[1] D. J. Gundlach, Y. Y. Lin, T. N. Jackson, S. F. Nelson, and D. G. Schlom, IEEE Electron Device Lett. **18**, 87 (1997).
[2] L. B. Lin, S. A. Jenekhe, R. H. Young, and P. M. Borsenberger, Appl. Phys. Lett. **70**, 2052 (1997).
[3] Y. Y. Lin, D. J. Gundlach, S. F. Nelson, and T. N. Jackson, IEEE Electron Device Lett. **18**, 606 (1997).
[4] B. Jaeckel, J. B. Sambur, and B. A. Parkinson, J. Appl. Phys. **103**, 063719 (2008).
[5] B. Jaeckel, J. Sambur, and B. A. Parkinson, J. Phys. Chem. C **113**, 1837 (2009).
[6] I. G. Hill, A. Rajagopal, A. Kahn, and Y. Hu, Appl. Phys. Lett. **73**, 662 (1998).
[7] W. R. Salaneck, K. Seki, A. Kahn, and J.-J. Pireaux, *Conjugated Polymer and Molecular Interfaces* (Marcel Dekker, New York, 2002).
[8] N. Karl and J. Marktanner, Mol. Cryst. Liq. Cryst. **355**, 149 (2001).
[9] A. J. Salih, S. P. Lau, J. M. Marshall, J. M. Maud, W. R. Bowen, N. Hilal, R. W. Lovitt, and P. M. Williams, Appl. Phys. Lett. **69**, 2231 (1996).
[10] E. V. Tsiper, Z. G. Soos, W. Gao, and A. Kahn, Chem. Phys. Lett. **360**, 47 (2002).
[11] S. F. Alvarado, L. Rossi, P. Muller, and W. Riess, Synth. Met. **122**, 73 (2001).
[12] N. Karl, K. H. Kraft, J. Marktanner, M. Munch, F. Schatz, R. Stehle, and H. M. Uhde, J. Vac. Sci. Technol. A **17**, 2318 (1999).
[13] F. Rudiono Kaneko and M. Takeuchi, Appl. Surf. Sci. **142**, 598 (1999).
[14] S. J. Kang, Y. Yi, K. Cho, K. Jeong, K. H. Yoo, and C. N. Whang, Synth. Met. **151**, 120 (2005).
[15] L. Gao, J. T. Sun, Z. H. Cheng, Z. T. Deng, X. Lin, S. X. Du, and H. J. Gao, Surf. Sci. **601**, 3179 (2007).
[16] C. Seidel, R. Ellerbrake, L. Gross, and H. Fuchs, Phys. Rev. B **64**, 195418 (2001).
[17] D. Wang, L. J. Wan, Q. M. Xu, C. Wang, and C. L. Bai, Surf. Sci. **478**, L320 (2001).
[18] C. B. France, P. G. Schroeder, J. C. Forsythe, and B. A. Parkinson, Langmuir **19**, 1274 (2003).
[19] C. B. France, P. G. Schroeder, and B. A. Parkinson, Nano Lett. **2**, 693 (2002).
[20] J. V. Barth, H. Brune, G. Ertl, and R. J. Behm, Phys. Rev. B **42**, 9307 (1990).
[21] P. G. Schroeder, C. B. France, J. B. Park, and B. A. Parkinson, J. Phys. Chem. B **107**, 2253 (2003).
[22] I. Horcas, R. Fernandez, J. M. Gomez-Rodriguez, J. Colchero, J. Gomez-Herrero, and A. M. Baro, Rev. Sci. Instrum. **78**, 013705 (2007).
[23] C. B. France and B. A. Parkinson, Langmuir **20**, 2713 (2004).
[24] K. Manandhar, T. Ellis, K. T. Park, T. Cai, Z. Song, and J. Hrbek, Surf. Sci. **601**, 3623 (2007).
[25] K. Manandhar, K. T. Park, S. Ma, and J. Hrbek, Surf. Sci. **603**, 636 (2009).

[26]I. Chizhov, G. Scoles, and A. Kahn, Langmuir **16**, 4358 (2000).
[27]M. D. Upward, P. H. Beton, and P. Moriarty, Surf. Sci. **441**, 21 (1999).
[28]M. Lackinger and M. Hietschold, Surf. Sci. **520**, L619 (2002).
[29]H. Luth, *Solid Surfaces, Interfaces, and Thin Films*, 4th ed. (Springer-Verlag, Berlin, 2001).
[30]J. J. Cox, S. M. Bayliss, and T. S. Jones, Surf. Sci. **433–435**, 152 (1999).
[31]S. Yim and T. S. Jones, Surf. Sci. **521**, 151 (2002).
[32]K. Oura, V. G. Lifshits, A. A. Saranin, A. V. Zotov, and M. Katayama, *Surf. Sci* (Springer-Verlag, Berlin, 2003).
[33]C. B. France and B. A. Parkinson, Appl. Phys. Lett. **82**, 1194 (2003).
[34]C. Wöll, S. Chiang, R. J. Wilson, and P. H. Lippel, Phys. Rev. B **39**, 7988 (1989).
[35]Z. H. Cheng, L. Gao, Z. T. Deng, Q. Liu, N. Jiang, X. Lin, X. B. He, S. X. Du, and H. J. Gao, J. Phys. Chem. C **111**, 2656 (2007).
[36]M. Koudia, M. Abel, C. Maurel, A. Bliek, D. Catalin, M. Mossoyan, J. C. Mossoyan, and L. Porte, J. Phys. Chem. B **110**, 10058 (2006).
[37]S. R. Forrest and P. E. Burrows, Supramol. Sci. **4**, 127 (1997).
[38]J. H. Kang and X. Y. Zhu, Appl. Phys. Lett. **82**, 3248 (2003).